Chapter 9

Conclusions and Recommendations for Future Research

The unsteady mid-span aerodynamics of an outlet stator blade row in a 1.5-stage low-speed axial compressor has been experimentally and numerically investigated. The compressor contained three blades rows: inlet guide vanes (IGV), rotor and stator. Two stator blade rows with characteristically different blade profiles were studied: one of British C4 section and a controlled diffusion (CD) blade with circular arc leading edge profile.

The influence of turbulence on the stator inlet flow was experimentally investigated. A turbulence generating grid placed upstream from the compressor section produced turbulence levels typical of those experienced by an embedded stage in a multi-stage compressor. Surveys made using a single-element hot-wire probe in the rotor–stator axial space were analysed to determine the pitchwise variation of velocity and turbulence. These results were compared with previous measurements made by Hughes [83] at low inlet turbulence level. The measurements of Hughes [83] showed that an interaction between IGV wakes and rotor wakes caused a periodic accumulation of low-energy rotor wake fluid, which lead to a significant pitchwise variation of turbulence properties. In the present study, increased inlet turbulence was found to accelerate IGV wake diffusion and significantly reduce IGV wake – rotor wake interaction. This resulted in a more circumferentially uniform velocity and turbulence field at entry to the stator blade row. Hence, numerical modelling must account for

the appreciable effect of free-stream turbulence in order to accurately predict wake dispersion and interaction processes.

The influence of inlet turbulence and blade row clocking on the transitional flow behaviour of a C4 stator was experimentally investigated with high inlet turbulence. Measurements from a row of surface mounted hot-film sensors on a stator blade were analysed to determine the temporal variation of turbulent intermittency and probability of calmed flow around the stator blade. These were compared with previous measurements made by Hughes [83] at low inlet turbulence level. Hughes [83] varied the turbulence level experienced by the stator by changing the relative alignment between IGV and stator blade rows. Aligning the IGV wake streets in the stator passage exposed the stator to a turbulence level between passing rotor wakes of about $0.5 - 1.0\%$. Immersing the stator blade row in IGV wake turbulence caused the stator to experience a turbulence level between wakes of about $2.0 - 3.0\%$. Hot-film measurements made by Hughes [83] at medium and high compressor loading showed that aligning the IGV wakes in the stator passage resulted in significant laminar or calmed flow between wake-induced transitional strips on the suction surface. Immersing the stator in IGV wake turbulence resulted in greater turbulent flow between wake-induced transitional strips. The flow on the stator blade surface at low loading was least influence by clocking.

The hot-film measurements at high inlet turbulence with the IGV wakes aligned in the stator passage were found to closely resemble the low inlet turbulence case with the stator blade row immersed in IGV wake turbulence. This similarity was observed in all compressor loading cases. This suggests that with appropriate alignment, a 1.5-stage axial compressor may be used to reliably predict the blade element behaviour of an embedded stage in a multi-stage machine. It also suggests that clocking effects between adjacent pairs of rotor or stator blade rows are likely to be more significant in flows with low levels of background turbulence, such as in the first few blade rows of a multi-stage machine. The fact that the transitional flow behaviour changed little between the two clocking cases in the high inlet turbulence tests is not surprising considering the circumferentially uniform turbulence level at entry to the stator blade row.

The flow around the CD stator was studied to determine the influence of leading edge velocity spikes on boundary layer behaviour. Measurements from a row of slow-response surface pressure tappings agreed well with numerical predictions from a

steady quasi three-dimensional flow solver, MISES. The relative height of the leading edge velocity spikes was strongly influenced by stator incidence. At design incidence, the spikes on both surfaces were of approximately equal height. Increasing incidence increased the height of the suction surface spike and decreased the height of the pressure surface spike. The MISES flow solver predicted transition on the suction surface at the leading edge spike in all incidence cases greater than and equal to design. In incidence cases less than design, the MISES flow solver predicted transition further along the suction surface following peak suction. Transition on the pressure surface was predicted at the leading edge in all cases, where it occurred through a leading edge separation bubble.

The unsteady transitional flow on the CD stator surface was also studied using an array of surface mounted hot-film sensors. The measurements were analysed to determine the temporal variation of ensemble average intermittency and probability of calming flow on the stator blade surface. A region of accelerating flow on the forward part of the suction surface had a stabilising effect on the boundary layer, with a significant portion of the surface in a laminar or transitional state. Wake-induced transitional strips formed on the suction surface, growing to eventually form continuously turbulent flow. The origin of these strips moved progressively upstream as loading was increased, reaching the leading edge velocity spike at high incidence. Examination of suction surface hot-film data showed that turbulent spots and other transitional flow disturbances periodically formed very close to the leading edge ($s^* \approx 0.05$). These disturbances were observed in all test cases, although their periodicity decreased as incidence and Reynolds number were reduced. These disturbances travelled along the surface with a mean convection velocity of about $0.7U$, often breaking down to form turbulent spots. Turbulent spots observed in the accelerating flow region had very low growth rates, and in some cases were relaminarised, either by acceleration or low Reynolds number effects. The flow on the pressure surface became turbulent at the leading edge in all cases except high incidence at low Reynolds number. The study shows that compressor blade leading edge profiles have a major influence on the boundary layer development over the whole surface.

The influence of incidence on CD stator losses was investigated. The flow field downstream from a stator blade element was surveyed over one a blade pitch using a three-hole probe and single-element hot-wire probe. The measurements were used to determine time-mean pressure loss coefficient and stator exit flow angle. These mea-

surements were compared with predictions from the MISES flow solver. Reasonable agreement was found at low incidence; but this deteriorated at design and positive incidence where the MISES flow solver predicted early transition at the suction surface leading edge and gave loss-estimates that were too high. The failure of the MISES flow solver to accurately predict performance was attributed to a combination of unsteady and three-dimensional effects.

The effect of passing rotor wakes on the stability of stator blade boundary layers was studied. Flow simulations using the unsteady quasi three-dimensional flow solver, UNSFLO, were used to interpret the unsteady laminar flow behaviour at the leading edge of both C4 and CD stators. Rotor wake chopping was predicted to generate periodic fluctuations in boundary layer skin friction at the leading edge of stator blades. The predicted flow behaviour agreed favourably with measurements from surface mounted hot-film sensors. The periodic decreases in skin friction on the suction surface coincide with increases in both momentum thickness Reynolds number and shape factor, which are both individually destabilising. The sign of the shear stress fluctuations was reversed on the pressure surface, indicating a stabilising effect. It is concluded that rotor wake chopping in compressors has a destabilising effect on the suction surface boundary layer and a stabilising effect on the pressure surface boundary layer.

Examination of hot-film data near the leading edge of both C4 and CD stator blades revealed a variety of transitional flow phenomena. Instability wave packets characteristic of T–S wave packets were observed to amplify and break down into turbulent spots. Disturbances characteristic of streaky structures occurring in bypass transition were also observed. Examination of suction surface disturbance trajectories points to the leading edge as the principal receptivity site for transitional flow phenomena occurring on the suction surface of both the C4 and CD blading. This contrasts markedly with the C4 pressure surface behaviour where transition can occur remote from leading edge flow perturbations. In this case, the boundary layer is more likely to be influenced by the wake fluid discharging onto the blade surface. It is concluded that wake chopping is likely have less influence on wake-induced transition occurring on the suction surface of turbine blades, due to the similarity of this flow regime to the compressor blade pressure surface situation.

The investigations described in this thesis have identified several areas for future research. One area of interest is how the unsteady transitional flow on the surface of

the CD stator is altered by rotor wake frequency. This could be achieved by replacing the existing rotor blade row with a blade row containing less blades, with longer chord length and increased blade loading. The stator blade row would then experience wake disturbances of larger magnitude at frequencies more typical of those found in modern aeroengine compressors. This would be expected to have an appreciable effect on transition between wake-induced turbulent strips as the pervasive effect of calming diminishes.

This thesis has shown that compressor blade leading edge profiles have a major influence on boundary layer development over the whole blade surface. Many questions remain unanswered regarding the optimisation of leading edge geometry. Further testing is required on blades with different leading edge profiles to determine the most significant design parameters influencing loss and performance. The wedge angle of circular arc leading edge profiles is likely to be important consideration. Larger wedge angles reduce the height of leading edge velocity spikes and increase the favourable pressure gradient near the leading edge, as seen in the study by Wheeler et al. [187]. This is likely to influence boundary layer behaviour at the leading edge.

Finally, there still insufficient data available on low Reynolds number boundary layer phenomena. Most research in the field of boundary layer transition tends to avoid the additional complexity of 'viscous effects' associated with low Reynolds number flows by testing at high Reynolds number. However, studies in low Reynolds number flows are essential in order to understand the boundary layer phenomena occurring at the leading edge of turbomachine blades.

Appendix A

Stator Blade Instrumentation

A.1 C4 Stator Blade Instrumentation

Blade Surface Pressure Tappings

Two stator blades were instrumented with pressure tappings as detailed in the previous study of Solomon [154]. Each blade contained 14 tubes oriented in the spanwise direction. Pressure tappings were drilled completely though the blade (and also through these tubes) at several spanwise distances. This allowed surface pressure measurements of either blade surface at several spanwise positions by sealing unused tappings with tape. Solomon [154] surveyed the mid-span pressure distribution by sealing all but the mid-span suction surface tappings on one blade and all but the mid-span pressure tappings on the other blade.

Solomon [154] later removed the blade used for pressure surface measurements, replacing it with a blade instrumented with an array of surface mounted hot-film sensors (described in the following section). Consequently, only pressure measurements of the suction surface were made in the present study. The tapping locations for this blade are indicated on a mid-span blade profile in Fig. A.1 and tabulated data is given in Table A.1.

Surface Mounted Hot-Film Sensors

One stator blade was instrumented with an array of surface mounted hot-film sensors as described in previous studies by Solomon [154]. Detail of the sensor array and manufacture is given in Section 6.5.1. The sensor locations are shown on a mid-span blade profile in Fig. A.1 and tabulated data is given in Table A.2.

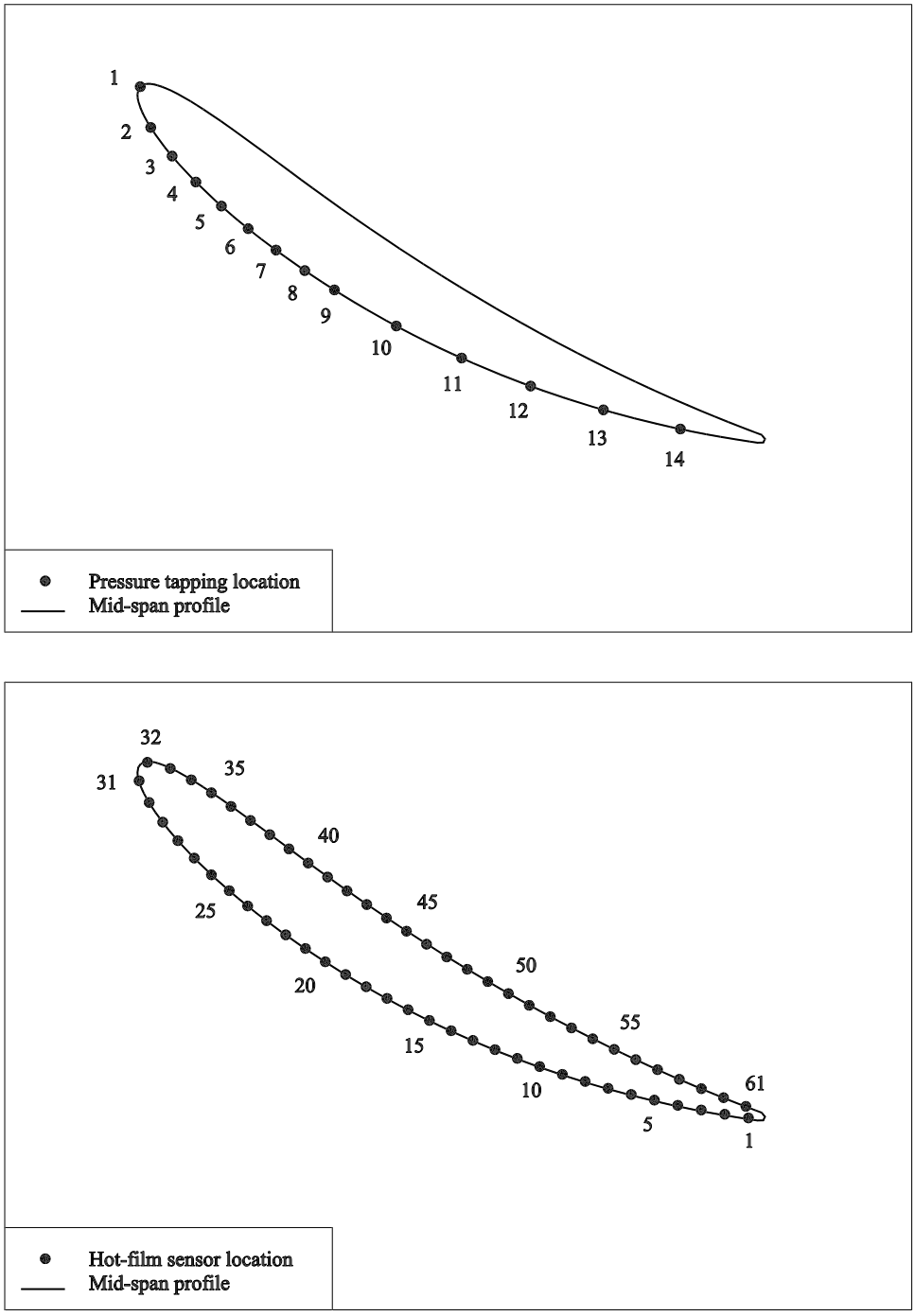

Figure A.1: Mid-span pressure tapping locations of C4 stator blade (top) and mid-span hot-film sensor locations of C4 stator blade (bottom)

Suction Surface				
#	x^*	s^*	x (mm)	y (mm)
1	0.0000	0.0000	0.00	0.00
2	0.0158	0.0580	1.05	4.22
3	0.0505	0.1067	3.35	7.33
4	0.0900	0.1556	5.97	10.17
5	0.1330	0.2048	8.82	12.84
6	0.1787	0.2546	11.85	15.36
7	0.2265	0.3047	15.02	17.76
8	0.2759	0.3552	18.30	20.04
9	0.3269	0.4058	21.68	22.20
10	0.4327	0.5074	28.70	26.14
11	0.5425	0.6089	35.98	29.55
12	0.6547	0.7095	43.42	32.40
13	0.7681	0.8087	50.94	34.68
14	0.8809	0.9056	58.42	36.43

Table A.1: Mid-span pressure tapping locations of C4 stator blade suction surface. All coordinates are relative to the geometrical blade leading edge defined as the intersection of the leading edge and camber line ($x = y = x^* = s^* = 0$). $x^* = x/c_x$ is dimensionless axial distance. $c_x = c\cos(\xi)$ is the axial projection of chord length. $s^* = s/s_{max}$ is dimensionless surface length. $c = 76.2$ mm and $s_{max} = 79.23$ mm (adapted from Solomon [154])

Suction Surface					Pressure Surface				
#	x^*	s^*	x (mm)	y (mm)	#	x^*	s^*	x (mm)	y (mm)
1	0.9730	0.9840	64.53	37.48	32	0.0107	0.0102	0.71	-0.29
2	0.9351	0.9519	62.02	37.09	33	0.0473	0.0435	3.14	0.37
3	0.8975	0.9199	59.52	36.64	34	0.0810	0.0768	5.37	1.58
4	0.8599	0.8878	57.03	36.14	35	0.1132	0.1101	7.51	2.95
5	0.8225	0.8557	54.55	35.59	36	0.1446	0.1434	9.59	4.40
6	0.7854	0.8237	52.09	34.99	37	0.1757	0.1767	11.65	5.89
7	0.7483	0.7916	49.63	34.33	38	0.2066	0.2100	13.70	7.40
8	0.7117	0.7596	47.20	33.61	39	0.2373	0.2433	15.74	8.91
9	0.6750	0.7275	44.77	32.85	40	0.2681	0.2766	17.78	10.41
10	0.6389	0.6955	42.37	32.03	41	0.2992	0.3099	19.84	11.90
11	0.6030	0.6634	39.99	31.16	42	0.3304	0.3432	21.91	13.37
12	0.5672	0.6313	37.62	30.23	43	0.3619	0.3765	24.00	14.82
13	0.5320	0.5993	35.28	29.25	44	0.3935	0.4098	26.10	16.25
14	0.4970	0.5672	32.96	28.22	45	0.4255	0.4431	28.22	17.65
15	0.4623	0.5352	30.66	27.13	46	0.4576	0.4764	30.35	19.03
16	0.4281	0.5031	28.39	25.99	47	0.4900	0.5097	32.50	20.38
17	0.3943	0.4711	26.15	24.79	48	0.5228	0.5430	34.67	21.70
18	0.3610	0.4390	23.94	23.55	49	0.5556	0.5763	36.85	23.00
19	0.3281	0.4069	21.76	22.25	50	0.5888	0.6096	39.05	24.28
20	0.2955	0.3749	19.60	20.90	51	0.6221	0.6429	41.26	25.52
21	0.2637	0.3428	17.49	19.49	52	0.6557	0.6762	43.49	26.73
22	0.2322	0.3108	15.40	18.04	53	0.6897	0.7095	45.74	27.92
23	0.2014	0.2787	13.36	16.53	54	0.7238	0.7428	48.00	29.08
24	0.1713	0.2467	11.36	14.97	55	0.7581	0.7761	50.28	30.20
25	0.1417	0.2146	9.40	13.35	56	0.7927	0.8094	52.57	31.29
26	0.1132	0.1825	7.51	11.66	57	0.8275	0.8427	54.88	32.35
27	0.0858	0.1505	5.69	9.89	58	0.8625	0.8760	57.20	33.38
28	0.0596	0.1184	3.95	8.03	59	0.8978	0.9093	59.54	34.37
29	0.0353	0.0864	2.34	6.07	60	0.9332	0.9426	61.89	35.33
30	0.0136	0.0543	0.90	3.98	61	0.9689	0.9759	64.26	36.25
31	-0.0026	0.0223	-0.17	1.68					

Table A.2: Mid-span hot-film sensor locations of C4 stator blade. All coordinates are relative to the geometrical blade leading edge defined as the intersection of the leading edge and camber line ($x = y = x^* = s^* = 0$). $x^* = x/c_x$ is dimensionless axial distance. $c_x = c\cos(\xi)$ is the axial projection of chord length. $s^* = s/s_{max}$ is dimensionless surface length. $c = 76.2$ mm, $s_{max} = 79.23$ mm on the suction surface and $s_{max} = 76.27$ on the pressure surface (adapted from Solomon [154])

A.2 CD Stator Blade Instrumentation

Blade Surface Pressure Tappings

One CD stator blade was instrumented with 39 pressure tappings as described in Section 7.5.2. A single row of pressure tappings at mid-span were drilled according to a CAD model of the blade: the same model used for manufacturing the blade row. The pressure tapping locations obtained from the CAD model are shown on a mid-span profile in Fig. A.2 and tabulated data is given in Table A.3.

Surface Mounted Hot-Film Sensors

One stator was instrumented with an array of surface mounted hot-film sensors. Information of the array and manufacture is given in Section 7.6.1. The centre position of each sensor was measured using a telescope mounted on a stand with vernier scale. These measurements were referenced against a CAD model of the stator blade to confirm the sensor positions. This approach was estimated to give the position of each sensor centre within ± 0.05 mm (sensor width was 0.2 mm). The sensor locations are indicated on a mid-span profile in Fig. A.2 and tabulated data is given in Table A.4.

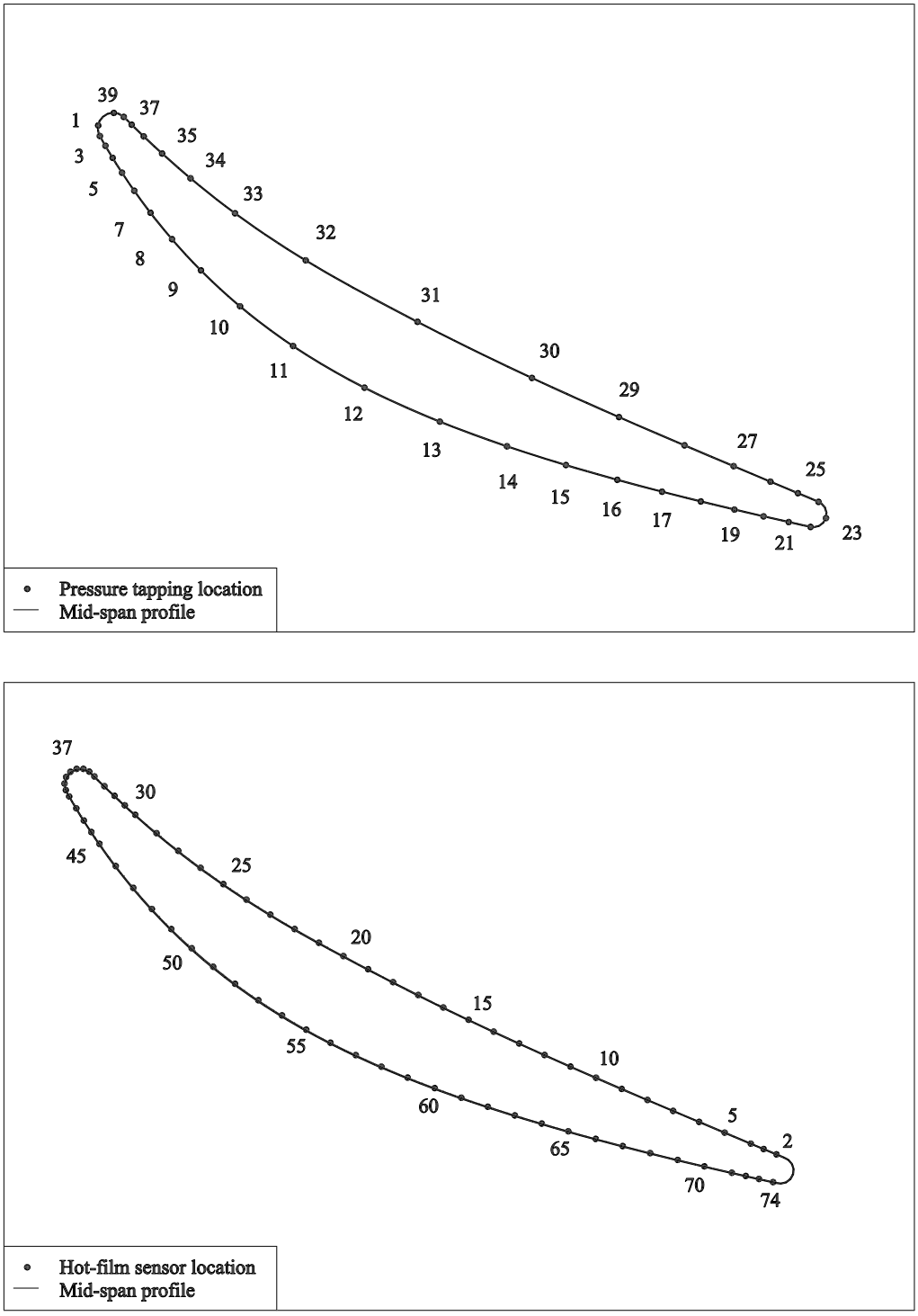

Figure A.2: Mid-span surface pressure tapping locations of CD stator blade (top) and mid-span hot-film sensor locations of CD stator blade (bottom)

Suction Surface					Pressure Surface				
#	x^*	s^*	x (mm)	y (mm)	#	x^*	s^*	x (mm)	y (mm)
1	-0.0076	0.0124	-1.02	1.69	23	1.0000	1.0000	132.94	73.91
2	-0.0054	0.0249	-0.71	3.63	24	0.9880	0.9763	131.56	70.94
3	0.0024	0.0377	0.31	5.43	25	0.9595	0.9501	127.78	69.35
4	0.0123	0.0536	1.64	7.65	26	0.9215	0.9146	122.71	67.22
5	0.0253	0.0734	3.37	10.37	27	0.8707	0.8669	115.94	64.37
6	0.0423	0.0982	5.63	13.70	28	0.8027	0.8037	106.90	60.54
7	0.0647	0.1295	8.61	17.75	29	0.7122	0.7186	94.84	55.34
8	0.0944	0.1682	12.57	22.61	30	0.5919	0.6055	78.83	48.14
9	0.1344	0.2165	17.90	28.35	31	0.4337	0.4536	57.75	37.81
10	0.1884	0.2768	25.09	34.95	32	0.2792	0.3020	37.18	26.50
11	0.2617	0.3517	34.85	42.26	33	0.1815	0.2010	24.17	17.85
12	0.3604	0.4459	47.99	49.93	34	0.1200	0.1337	15.97	11.41
13	0.4646	0.5395	61.87	56.17	35	0.0807	0.0890	10.74	6.85
14	0.5574	0.6206	74.22	60.71	36	0.0552	0.0591	7.36	3.69
15	0.6388	0.6908	85.07	64.17	37	0.0386	0.0391	5.14	1.55
16	0.7099	0.7516	94.53	66.88	38	0.0276	0.0258	3.68	0.11
17	0.7717	0.8041	102.76	69.07	39	0.0140	0.0129	1.86	-0.62
18	0.8253	0.8494	109.89	70.86					
19	0.8717	0.8938	116.08	72.35					
20	0.9120	0.9227	121.44	73.61					
21	0.9468	0.9531	126.08	74.66					
22	0.9770	0.9778	130.10	75.55					
23	1.0000	1.0000	132.94	73.91					

Table A.3: Mid-span pressure tapping locations of CD stator blade. All coordinates are relative to the geometrical blade leading edge defined as the intersection of the leading edge and camber line ($x = y = x^* = s^* = 0$). $x^* = x/c_x$ is dimensionless axial distance. $c_x = c\cos(\xi)$ is the axial projection of chord length. $s^* = s/s_{max}$ is dimensionless surface length. $c = 152.4$ mm and $s_{max} = 162.1$ mm on the suction surface and $s_{max} = 154.8$ mm on the pressure surface

Suction Surface					Pressure Surface				
#	x^*	s^*	x (mm)	y (mm)	#	x^*	s^*	x (mm)	y (mm)
37	-0.0005	0.0005	-0.07	0.05	2	0.9737	0.9652	129.91	70.34
38	-0.0064	0.0083	-0.85	1.02	3	0.9558	0.9485	127.53	69.35
39	-0.0087	0.0161	-1.16	2.23	4	0.9380	0.9319	125.15	68.35
40	-0.0068	0.0239	-0.91	3.46	5	0.9024	0.8985	120.39	66.35
41	-0.0024	0.0316	-0.32	4.57	6	0.8667	0.8652	115.64	64.35
42	0.0074	0.0476	0.99	6.78	7	0.8311	0.8319	110.89	62.34
43	0.0175	0.0635	2.34	8.98	8	0.7955	0.7985	106.14	60.33
44	0.0280	0.0794	3.74	11.14	9	0.7600	0.7652	101.40	58.30
45	0.0389	0.0953	5.19	13.27	10	0.7245	0.7319	96.66	56.25
46	0.0616	0.1271	8.22	17.44	11	0.6891	0.6986	91.94	54.18
47	0.0858	0.1589	11.45	21.46	12	0.6538	0.6652	87.22	52.09
48	0.1113	0.1908	14.85	25.34	13	0.6185	0.6319	82.52	49.96
49	0.1381	0.2226	18.43	29.05	14	0.5834	0.5986	77.84	47.80
50	0.1663	0.2544	22.19	32.59	15	0.5484	0.5652	73.17	45.60
51	0.1957	0.2863	26.10	35.94	16	0.5136	0.5319	68.53	43.36
52	0.2262	0.3181	30.17	39.11	17	0.4790	0.4986	63.90	41.07
53	0.2577	0.3499	34.39	42.09	18	0.4445	0.4653	59.30	38.74
54	0.2903	0.3817	38.73	44.88	19	0.4102	0.4319	54.72	36.36
55	0.3236	0.4136	43.18	47.49	20	0.3760	0.3986	50.16	33.95
56	0.3577	0.4454	47.73	49.92	21	0.3420	0.3653	45.62	31.49
57	0.3925	0.4772	52.36	52.18	22	0.3083	0.3319	41.13	28.97
58	0.4277	0.5090	57.07	54.29	23	0.2750	0.2986	36.69	26.34
59	0.4634	0.5409	61.83	56.27	24	0.2422	0.2653	32.32	23.60
60	0.4997	0.5729	66.67	58.14	25	0.2101	0.2320	28.03	20.73
61	0.5361	0.6047	71.52	59.89	26	0.1786	0.1986	23.83	17.74
62	0.5727	0.6365	76.41	61.55	27	0.1479	0.1653	19.73	14.61
63	0.6095	0.6684	81.32	63.12	28	0.1179	0.1320	15.73	11.35
64	0.6465	0.7002	86.26	64.62	29	0.0887	0.0986	11.83	7.98
65	0.6837	0.7320	91.21	66.05	30	0.0744	0.0820	9.92	6.25
66	0.7209	0.7639	96.19	67.43	31	0.0603	0.0653	8.04	4.49
67	0.7583	0.7957	101.17	68.75	32	0.0463	0.0487	6.18	2.71
68	0.7958	0.8275	106.17	70.03	33	0.0326	0.0320	4.34	0.90
69	0.8333	0.8593	111.18	71.27	34	0.0257	0.0238	3.43	0.03
70	0.8709	0.8912	116.19	72.47	35	0.0173	0.0157	2.30	-0.50
71	0.9085	0.9230	121.22	73.64	36	0.0079	0.0076	1.05	-0.49
72	0.9274	0.9389	123.73	74.21					
73	0.9462	0.9548	126.25	74.78					
74	0.9651	0.9707	128.77	75.34					

Table A.4: Mid-span hot-film sensor locations of CD stator blade. All coordinates are relative to the geometrical blade leading edge defined as the intersection of the leading edge and camber line ($x = y = x^* = s^* = 0$). $x^* = x/c_x$ is dimensionless axial distance. $c_x = c\cos(\xi)$ is the axial projection of chord length. $s^* = s/s_{max}$ is dimensionless surface length. $c = 152.4$ mm and $s_{max} = 162.1$ mm on the suction surface and $s_{max} = 154.8$ mm on the pressure surface

Appendix B

Design of the Turbulence Grid

The turbulence grid was designed to produce turbulence properties at entry to the stator blade similar to those measured in multi-stage compressors by Camp and Shin [18]. This study showed that multi-stage compressors operate with a typical background turbulence intensity of 4% and integral length scale of $\Lambda_x/c = 0.06$.

The turbulence grid design was based on the data of Roach [135], which gives test data and empirical correlations for pressure loss, turbulence intensity and integral length scale downstream from several types of grids and arrays of parallel bars.

The pressure loss resulting from the grid was also an important design consideration. It had to be sufficiently small to allow the compressor to operate at the same operating points used in previous studies to allow comparisons between measurements made both with and without the grid. A circular cross section was chosen since it gives a lower pressure loss for a given size than a rectangular section (see Roach [135]).

The final design consisted of 38 brass rods spanning radially between two brass rings. Each ring was constructed by rolling a rectangular brass section (19.3 mm by 3.2 mm) to fit firmly against the compressor hub and casing walls. Countersunk holes were drilled at evenly spaced intervals around the ring. Each rod was placed between the inner and outer rings and fastened at each end by a countersunk screw. All rods were a standard diameter of 7.84 mm. The final assembly was located in the compressor approximately 175 mm upstream from the IGV blade row. Each ring was fixed to the hub and casing walls by 4 countersunk screws.

The following sections provide detail of the predicted turbulence properties and pressure loss resulting from the grid.

B.1 Turbulence Intensity

Roach [135] provides correlations for the one-dimensional variation of turbulence properties with downstream distance from turbulence grids. The turbulence intensity behind a parallel array of round rods may be described by

$$Tu = 80 \left[\frac{x}{D}\right]^{-\frac{5}{7}} \tag{B.1.1}$$

where D is the rod diameter, x is the distance downstream and Tu is the corresponding turbulence intensity expressed as a percentage.

The streamwise distances from the grid to the IGV and stator blade rows were estimated from time-mean particle trajectories These were determined to be 187 mm and 493 mm respectively (taken as variable x in Eq. (B.1.1). Substituting these values into Eq. (B.1.1) yields the following turbulence intensity at entry the IGV and stator blade rows (using a rod diameter of $D = 7.94$ mm)

$$\begin{aligned} (Tu)_{IGV} &= 8.7\% \\ (Tu)_{stator} &= 4.3\% \end{aligned} \tag{B.1.2}$$

B.2 Integral Length Scale

Roach [135] correlates the integral length of turbulence downstream from grids and parallel arrays of bars as

$$\frac{\Lambda_x}{c} = \left(\frac{D}{c}\right) 0.2 \sqrt{\frac{x}{D}} \tag{B.2.1}$$

Substituting the estimated distances from B.1 gives

$$\begin{aligned} (\Lambda_x/c)_{IGV} &= 0.049 \\ (\Lambda_x/c)_{stator} &= 0.081 \end{aligned} \tag{B.2.2}$$

where c is the chord length of the CD stator

B.3 Pressure Loss

Roach [135] also defines a pressure loss coefficient for grids and arrays of parallel bars.

This may be written as

$$k_g = \frac{\Delta P}{0.5\rho V^2} = A\left(\frac{1}{\beta^2} - 1\right)^B \tag{B.3.1}$$

where the β is the grid porosity, and A, B are empirical constants. Using the test data for a parallel array of cylindrical rods with spacing equal to the mid-span spacing of the turbulence grid gives $\beta = 0.89$, $A = 0.53$ and $B = 1$ This gives a loss factor of $k_g = 0.13$.

The reduction in compressor flow coefficient resulting from the pressure loss associated with the grid was obtained from the performance measurements made by Oliver [122]. The 'system resistance' resulting from the natural pressure loss of the research compressor varies with throttle opening. The limiting case of maximum flow coefficient occurs at large throttle opening ($\phi = 0.90$ at 20 inches throttle opening). The system loss corresponding to this operating point may be assumed equal to difference in total pressure across the compressor. Expressing this loss term in the same form as Eq. (B.3.1) results in $k_{s_{no-grid}} = 0.50$. The system resistance including the turbulence grid is $k_{s_{grid}} = k_{s_{no-grid}} + k_g = 0.63$ Matching this result to the compressor characteristic given in Oliver [122] gives a new operating point of $\phi = 0.86$, which allows operation at the high flow coefficient test case $\phi = 0.84$. The measured change in flow coefficient at a throttle setting of 22 inches was $\Delta\phi = -0.036$ (C4 stator, $Re_c = 120000$) compares well with the predicted value of $\Delta\phi = -0.04$.

Appendix C

Compressor Reference Pressure

Prior to installation of the turbulence grid, the dynamic pressure at inlet to the compressor was measured using a pitot-static tube positioned between the inlet contraction and the IGV blade row. However, introducing a turbulence grid upstream from this reference would affect its accuracy, thus requiring a new reference pressure.

A CFD investigation of the inlet contraction revealed that a large pressure differential develops across the inner and outer surfaces. The study indicated the position corresponding to the largest differential and that that pressure tappings placed at this location would not be altered by a downstream grid.

Following this investigation, static ring tappings were placed on the inner and outer surfaces of the inlet contraction. The resulting pressure differential was calibrated against the existing pitot-static tube reference prior to installation of the turbulence grid. The results were used to determine a new method for calculating the compressor inlet dynamic pressure from the measured pressure differential across the inlet contraction.

This Appendix details the CFD investigation of the inlet contraction and presents the calibration of the new reference for determining the compressor inlet dynamic pressure.

C.1 Model of Research Compressor Inlet Contraction

A computational study was undertaken to investigate the flow through the inlet contraction. Commercial CFX software (AEA Technology Inc) was used for the analysis. The software included tools for creating geometry, meshing, solving and post-processing. The following sections describe the CFD model and present the key results.

Model Domain

The domain of the CFD model may be described by several regions of flow: entry to the inlet screen, between the shell and core pieces of the contraction, and through the annular section corresponding to the working section. The compressor was not modelled since the objective of the study was to determine the influence of the grid on the inlet flow. The flow through the model was assumed circumferentially uniform and axisymmetrical. These assumptions allowed the model size to be reduced to one quarter of full size by using symmetry planes in the axial–radial directions. A rendered view of the model geometry is shown in the top part of Fig. C.1.

Boundary Conditions

Quadratic source terms were included in the momentum equations to represent pressure losses resulting from the inlet screen and turbulence grid. The source terms were applied to the relevant direction components of the momentum equations. For example a loss in the x-direction the term may be expressed by

$$k^* = \frac{1}{U^2}\frac{dP}{dx} = \frac{\rho k}{2\Delta x} \tag{C.1.1}$$

where the k is the conventional loss coefficient of the form given in Eq. (B.3.1). The pressure loss coefficients were estimated from correlations given by Roach [135]. The pressure loss terms could be removed by simply setting the loss term to zero.

The mass flow rate through the model was fixed by specifying a constant velocity at exit. This corresponded to medium compressor load $\phi = 0.675$ at $Re_c = 120000$ ($V_a \approx 16$ m/s). A constant total pressure at Standard Temperature and Pressure was applied at the model inlet.

Computational Mesh

The mesh consisted of prismatic elements (pentahedral) attached to all wall surfaces and tetrahedral elements in the remaining free-stream flow. The solver did not allow use of thin surfaces to represent the inlet screen and turbulence grid. Instead, these were modelled by thin layer of tetrahedral elements. The final mesh contained a total of approximately $1.4(10)^6$ elements.

Model Parameters

The CFX model parameters are summarised in Table C.1. Convergence was assumed to have occurred when all the flow residuals had reduced by at least 3 orders of magnitude.

Parameter	**Setting**
Solver	3-D, Steady-state, Incompressible
Advection Scheme	High Accuracy Second-Order
Fluid properties	Incompressible, Isothermal Air at STP
Turbulent Closure	Standard $k-\epsilon$
Wall Functions	Scalable

Table C.1: Table of CFX model parameters

Solution Results

The calculated y^+ values for the wall functions were within the range $5 \leq y^+ \leq 110$. This is close to the range of $20 \leq y^+ \leq 100$ recommended in the CFX documentation [89]. The lowest values occurred on the outside facing surfaces of the core and casing pieces in regions of slowly moving flow. This not considered to adversely effect the solution results.

An inlet pressure coefficient may be defined as

$$C_{Pinl} = \frac{2(P_{inlet} - p)}{\rho V_{out}^2} \tag{C.2.1}$$

where P_{inlet} is the total pressure at inlet to the model, p is the static pressure and $\frac{1}{2}\rho(V_{out})^2$ is the average dynamic pressure at the model outlet downstream from the position of the turbulence grid.

The top part of Fig. C.1 shows the pressure coefficient defined by Eq. (C.2.1) on a radial–axial section through the intake contraction. A local region of low pressure is observed close to shell piece as the flow is turned 90°. This contrasts with the pressure distribution on the core piece where the pressure remains higher and the gradient is much lower. Static pressure drops are observed across both the inlet screen and the turbulence grid.

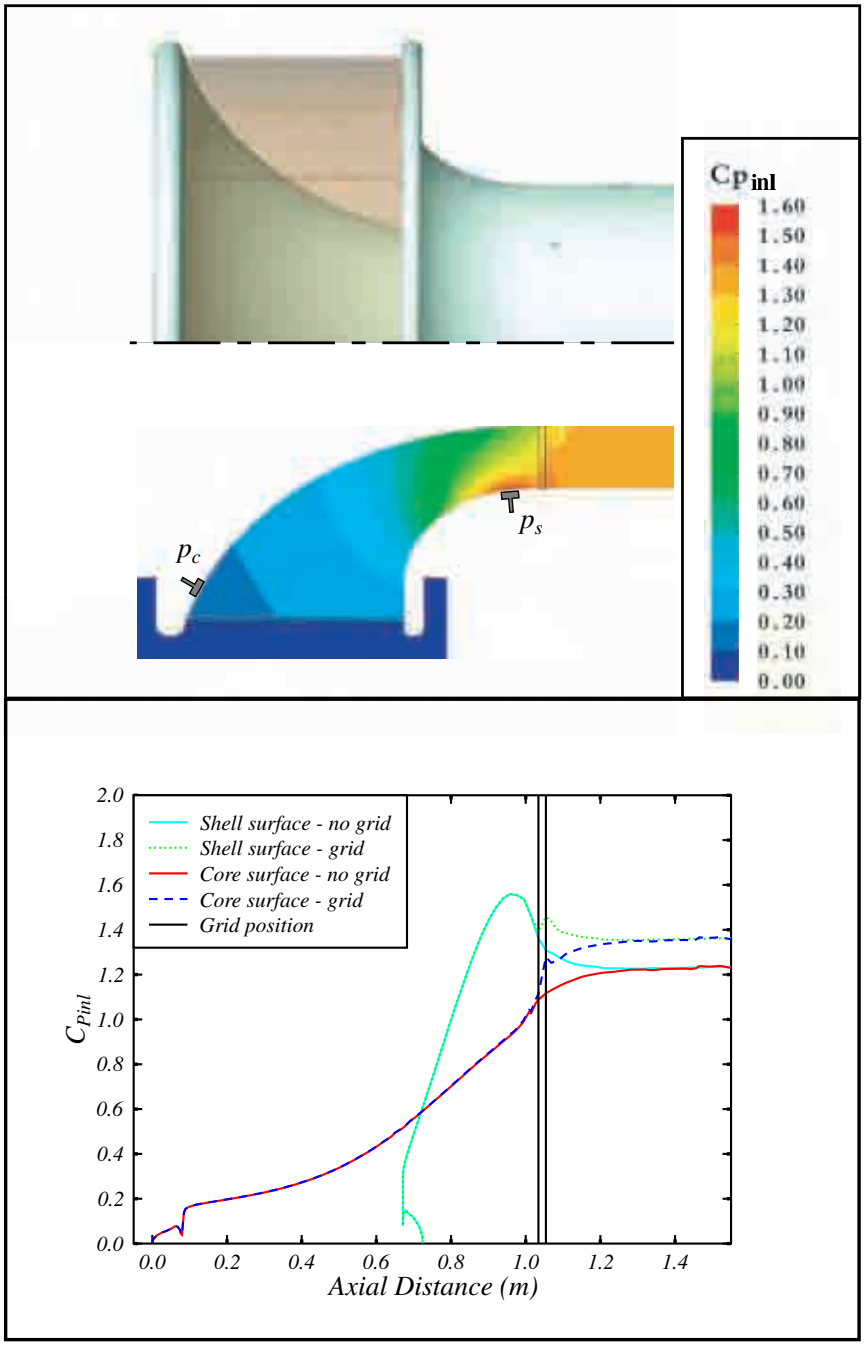

Figure C.1: Numerical simulation of research compressor inlet contraction (CFX). Rendered view of intake model (top) with corresponding contours of pressure coefficient on a radial plane and pressure coefficient of intake surfaces with and without loss terms for the grid included (bottom)

The bottom part of Fig. C.1 shows variation of pressure coefficient along each surface with axial distance. The axial coordinate is consistent with the top part of the figure. Solution results are presented for both cases with and without inclusion of the loss term representing the turbulence grid. The results show the surface pressure distribution of the intake contraction is not is not significantly influenced by the pressure drop associated with the turbulence grid. These results suggest that the static pressure differential across the inlet contraction may be calibrated to determine the inlet dynamic pressure at compressor inlet.

C.2 Calibration of Inlet Contraction

A new method was developed for estimating the compressor inlet dynamic pressure based on the static pressure differential across the inlet contraction. The method had to be sufficiently simple to be calculated 'real-time' by the computer controlling the wind tunnel. The method is summarised below.

The contraction pressure coefficient may be defined by

$$C_{Pcon} = \frac{2(p_c - p_s)}{\rho(V_a)^2} \tag{C.2.1}$$

where the static pressures p_c and p_s shown in Fig. C.1 are measured by ring tappings. The dynamic pressure at inlet to the compressor ($\frac{1}{2}\rho(V_a)^2$) is measured by the reference pitot-static tube at inlet to the compressor. The contraction pressure coefficient (C_{Pcon}) remains approximately constant at 1.3 for varying compressor inlet Reynolds number (Re_a) and flow coefficient (ϕ): this first-order approximation allows the compressor inlet velocity (V_a') to be estimated from

$$V_a' = \sqrt{\frac{2(p_c - p_s)}{1.3\rho}} \tag{C.2.2}$$

This allows the approximate values of inlet Reynolds number and flow coefficient to be estimated from

$$Re_a' = \frac{Re_c(V_a')}{U_{mb}} \tag{C.2.3}$$

$$\phi' = \frac{Re_a'}{Re_c} = \frac{V_a'}{U_{mb}} \tag{C.2.4}$$

These values may be used to correct the contraction pressure for Reynolds number

and flow coefficient effects. The corrected inlet contraction coefficient may be written as

$$C'_{Pcon} = 1.352 - 8.99 Re_a'^{-0.469} + \Delta \tag{C.2.5}$$

where Δ is a flow coefficient correction given by

$$\Delta = \begin{cases} 2.69\phi'^2 - 3.93\phi + 1.431, & \phi \leq 0.730 \\ 0, & \phi \geq 0.730 \end{cases} \tag{C.2.6}$$

The final values of compressor inlet velocity and flow coefficient are determined from Eq. (C.2.5). This may be expressed as

$$V_a = \sqrt{\frac{2(P_c - P_s)}{\rho C'_{Pcon}}} \tag{C.2.8}$$

$$\phi = \frac{V_a}{U_{mb}} \tag{C.2.9}$$

Figure C.2 compares the new method with measurements from the original reference for both C4 and CD stators. Although there is considerable scatter in the data, the flow coefficient calculated using the new method is within 1% of the existing reference over the range of flow coefficients used for testing in this thesis ($0.6 < \phi < 0.84$).

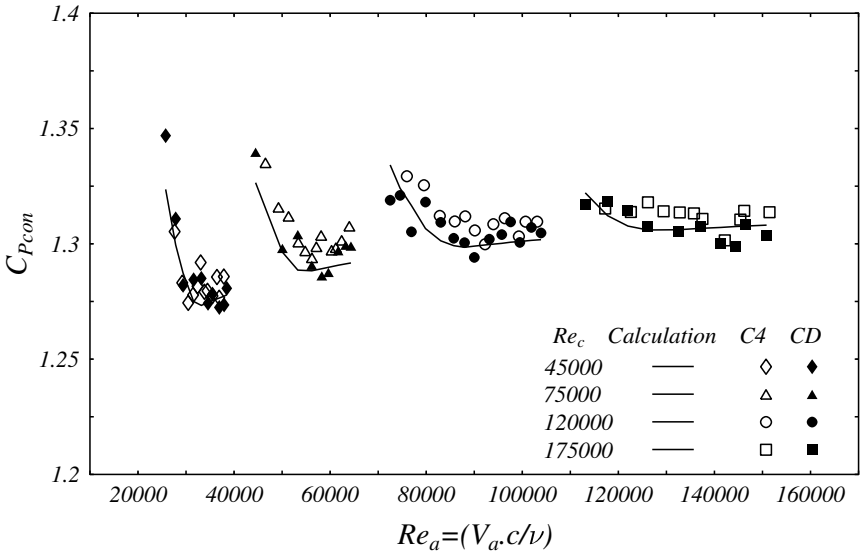

Figure C.2: Calibration of research compressor contraction pressure coefficient without turbulence grid installed (markers). Lines indicate flow coefficient calculated by the method presented above

Bibliography

[1] B. J. Abu Ghannam and R. Shaw. Natural transition of boundary layers — The effects of pressure gradient and flow history. *Journal of Mechanical Engineering Science*, **22**(5):213–228, 1980.

[2] M. Alam and N. D. Sandham. Direct numerical simulation of 'short' laminar separation bubbles with turbulent reattachment. *Journal of Fluid Mechanics*, **410**:1–28, 2000.

[3] S. J. Andrews. Tests related to the profile shape and camber-line on compressor cascade performance. Aeronautical Research Council (ARC) Reports and Memoranda 2743, UK, 1949.

[4] R. L. Anthony, T. V. Jones, and J. E. LaGraff. High frequency surface flux imaging of bypass transition. *ASME Journal of Turbomachinery*, **127**:241–250, 2005.

[5] A. V. Arena and T. J. Mueller. Laminar separation, transition, and turbulent reattachment near the leading edge of airfoils. *AIAA Journal*, **18**:747–753, 1980.

[6] M. Asai, M. Minagawa, and M. Nishioka. The instability and breakdown of a near-wall low-speed streak. *Journal of Fluid Mechanics*, **455**:289–314, 2002.

[7] M. A. Badri Narayanan and V. Ramjee. On the criteria for reverse transition in a two-dimensional boundary layer flow. *Journal of Fluid Mechanics*, **35**(2): 225–241, 1969.

[8] A. A. Bakchinov, K. J. A. Westin, V. V. Kozlov, and P. H. Alfredsson. Experiments on localized disturbances in a flat plate boundary layer. Part 2. Interaction between localized disturbances and TS-waves. *European Journal of Mechanics B/Fluids*, **17**(6):847–873, 1998.

[9] M. F. Blair. Boundary layer transition in accelerating flows with intense freestream turbulence: Part 1 — Disturbances upstream of transition onset. *Journal of Fluid Mechanics*, **114**:313–321, 1992.

[10] M. F. Blair. Boundary layer transition in accelerating flows with intense freestream turbulence: Part 2 — The zone of intermittent turbulence. *Journal of Fluid Mechanics*, **114**:322–332, 1992.

[11] F. G. Blight and W. Howard. Tests on four aerofoil cascades. Part 1: Deflection, drag and velocity distribution. Aeronautical Research Laboratories (ARL) Report E.74, Australia, 1952.

[12] A. V. Boiko, G. R. Grek, A. V. Dovgal, and V. V. Kozlov. *The Origin of Turbulence in Near-Wall Flows*. Springer, Berlin, 2002.

[13] A. V. Boiko, K. J. A. Westin, B. G. B. Klingmann, V. V. Kozlov, and P. H. Alfredsson. Experiments in a boundary layer subjected to free stream turbulence. Part 2. The role of TS-waves in the transition process. *Journal of Fluid Mechanics*, **281**:219–245, 1994.

[14] C. Bourassa, F. O. Thomas, and R. C. Nelson. Experimental investigation of turbulent boundary layer relaminarization with application to high-lift systems — preliminary results. In *Proc. AIAA Applied Aerodynamics Conference, Paper 2000-4017*, Denver, Colorado, USA, 2000.

[15] P. J. Boxhall. *Unsteady Flow Phenomena in an Axial-Flow Compressor*. MEngSc Thesis, University of Tasmania, Australia, 1971.

[16] L. Brandt, P. Schlatter, and D. S. Henningson. Transition in boundary layers subject to free-stream turbulence. *Journal of Fluid Mechanics*, **517**:167–198, 2004.

[17] R. E. Britter, J. C. R. Hunt, and J. C. Mumford. The distortion of turbulence by a circular cylinder. *Journal of Fluid Mechanics*, **92**(2):269–301, 1979.

[18] T. R. Camp and H. W. Shin. Turbulence intensity and length scale measurements in multistage compressors. *ASME Journal of Turbomachinery*, **117**:38–46, 1995.

[19] T. Cebeci and A. M. O. Smith. *Analysis of Turbulent Boundary Layers*. Academic Press, New York, 1974.

[20] K. K. Chen and N. A. Thyson. Extension of Emmons' Spot Theory to flows on blunt bodies. *AIAA Journal*, **9**:821–825, 1971.

[21] Y. Chow, O. Uzol, and J. Katz. Flow non-uniformities and turbulent "hot spots" due to wake-blade and wake-wake interactions in a multistage turbomachine. *ASME Journal of Turbomachinery*, **124**:553–563, 2002.

[22] J. Cohen, K. S. Breuer, and J. H. Haritondis. On the evolution of a wave packet in a laminar boundary layer. *Journal of Fluid Mechanics*, **225**:575–606, 1991.

[23] D. C. Collis and M. J. Williams. Two-dimensional convection from heated wires. *Journal of Fluid Mechanics*, **6**:357–384, 1959.

[24] N. A. Cumpsty. *Compressor Aerodynamics*. Longman Scientific and Technical, 1989.

[25] S. Deutsch and W. C. Zierke. The measurement of boundary layers on a compressor blade in cascade: Part 1 — A unique experimental facility. *ASME Journal of Turbomachinery*, **109**:520–526, 1987.

[26] S. Deutsch and W. C. Zierke. The measurement of boundary layers on a compressor blade in cascade: Part 2 — Suction surface boundary layers. *ASME Journal of Turbomachinery*, **110**:138–145, 1988.

[27] S. Deutsch and W. C. Zierke. The measurement of boundary layers on a compressor blade in cascade: Part 3 — Pressure surface boundary layers and the near wake. *ASME Journal of Turbomachinery*, **110**:146–152, 1988.

[28] S. Dhawan and R. Narasimha. Some properties of boundary layer flow during the transition from laminar to turbulent motion. *Journal of Fluid Mechanics*, **3**:418–436, 1957.

[29] Y. Dong and N. A. Cumpsty. Compressor blade boundary layers: Part 1 – Test facility and measurements with no incident wakes. *ASME Journal of Turbomachinery*, **112**:222–230, 1990.

[30] Y. Dong and N. A. Cumpsty. Compressor blade boundary layers: Part 2 — Measurements with incident wakes. *ASME Journal of Turbomachinery*, **112**: 231–240, 1990.

[31] D. J. Doorly and M. L. G. Oldfield. Simulation of the effects of shock wave passing on a turbine rotor blade. *ASME Journal of Turbomachinery*, **107**:998–1006, 1985.

[32] D. J. Doorly and M. L. G. Oldfield. Simulation of wake passing in a stationary turbine rotor cascade. *AIAA Journal of Propulsion and Power*, **1**(4):316–318, 1985.

[33] A. V. Dovgal and V. V. Kozlov. Influence of acoustic perturbations on the flow structure in a boundary layer with adverse pressure gradient. *Fluid Dynamics*, **18**(2):205–209, 1983.

[34] A. D'Ovidio, J. A. Harkins, and J. P. Gostelow. Turbulent spots in strong adverse pressure gradients. Part 2 — Spot propagation and spreading rates. ASME Paper 2001-GT-406, 2001.

[35] M. Drela. MISES implementation of modified Abu-Ghannam/Shaw transition criterion. Technical Report , Second Revision, MIT Aero-Astro, 1998.

[36] M. Drela and M. B. Giles. Viscous-inviscid analysis of transonic and low Reynolds number airfoils. *AIAA Journal*, **25**(10):1347–1355, 1987.

[37] M. Drela and H. Youngren. A user's guide to MISES 2.53. Technical report, MIT Computational Aerospace Sciences Laboratory, 1998.

[38] Y. Elazar and R. P. Shreeve. Viscous flow in a controlled diffusion compressor cascade with increasing incidence. *ASME Journal of Turbomachinery*, **112**:256–266, 1990.

[39] W. Elsner, S. Drobniak, S. Vilmin, and W. Piotrowski. Experimental analysis and prediction of wake-induced transition in turbomachinery. ASME Paper GT2004-53757, 2004.

[40] H. W. Emmons. The laminar-turbulent transition in a boundary layer — Part I. *Journal of Aerospace Sciences*, **18**(7):490–498, 1951.

[41] M. P. Escudier, A. Abdel-Hameed, M. W. Johnson, and C. J. Sutcliffe. Laminarisation and re-transition of a turbulent boundary layer subjected to a favourable pressure gradient. *Experiments in Fluids*, **25**:491–502, 1998.

[42] R. L. Evans. Turbulence and unsteadiness measurements downstream of a moving blade row. *ASME Journal of Engineering for Power*, **122**:131–139, 1975.

[43] R. E. Falco and C. P. Gendrich. The turbulence detection algorithm of Z. Zarić. In S. J. Kline and N. H. Afgan, editors, *Near-Wall Turbulence 1988 Zoran Zarić Memorial Conference*, pages 911–931. Hemisphere, 1990.

[44] K. Funazaki and Y. Kato. Studies on a blade leading edge separation bubble affected by periodic wakes: Its transitional behavior and boundary layer loss reduction. ASME Paper GT-2002-30221, 2002.

[45] K. Funazaki, K. Yamada, and Y. Kato. Studies on effects of periodic wake passing upon a blade leading edge separation bubble: Experimental investigation using a simple leading edge model. *ASME Journal of Turbomachinery*, **5B**:761–769, 2003.

[46] S. J. Gallimore, J. J. Bolger, N. A. Cumpsty, M. J. Taylor, P. I. Wright, and J. M. M. Place. The use of sweep and dihedral in multistage axial flow compressor blading: Part I: University research and methods development. *ASME Journal of Turbomachinery*, **124**(4):521–532, 2002.

[47] S. J. Gallimore, J. J. Bolger, N. A. Cumpsty, M. J. Taylor, P. I. Wright, and J. M. M. Place. The use of sweep and dihedral in multistage axial flow compressor blading: Part II : Low and high speed designs and test verification. *ASME Journal of Turbomachinery*, **124**(4):533–542, 2002.

[48] M. Gaster. The structure and behaviour of laminar separation bubbles. In *Proc. AGARD Conference No. 4. Separated Flows*, Rhode-Stain-Genese, Belgium, 1966.

[49] M. Giles. UNSFLO: A numerical method for the calculation of unsteady flow turbomachinery. Gas Turbine Laboratory (GTL) Report #205 , Massachusetts Institute of Technology, Cambridge, Massachusetts, USA, 1991.

[50] M. Giles and R. Haimes. Validation of a numerical method for unsteady flow calculations. *ASME Journal of Turbomachinery*, **115**:110–117, 1993.

[51] C. Gleyzes, J. Cousteix, and J. L. Bonnet. Theoretical and experimental study of low Reynolds number transitional separation bubbles. In T. Cebeci, editor, *Numerical and Physical Aspects of Aerodynamic Turbulent Flows II*, pages 173–192. Springer-Verlag, 1985.

[52] S. E. Gorrell, T. H. Okiishi, and W. W. Copenhaver. Stator-rotor interactions in a transonic compressor — Part 1: Effect of blade-row spacing on performance. *ASME Journal of Turbomachinery*, **125**(2):328–335, 2003.

[53] J. P. Gostelow, A. R. Blunden, and G. J. Walker. Effects of free-stream turbulence and adverse pressure gradients on boundary layer transition. *ASME Journal of Turbomachinery*, **116**:392–404, 1994.

[54] J. P. Gostelow, N. Melwani, and G. J. Walker. Effects of streamwise pressure gradient on turbulent spot development. *ASME Journal of Turbomachinery*, **118**:737–743, 1996.

[55] J. P. Gostelow and R. L. Thomas. Response of a laminar separation bubble to an impinging wake. *ASME Journal of Turbomachinery*, **127**(1):35–42, 2005.

[56] J. P. Gostelow and R. L. Thomas. Interactions between propagating wakes and flow instabilities in the presence of a laminar separation bubble. ASME Paper GT2006-91193, 2006.

[57] W. Gracey. Wind-tunnel investigation of a number of total-pressure tubes at high angles of attach — Subsonic, transonic and supersonic speeds. Technical Report 1303, NACA, 1956.

[58] C. Haldeman, M. Dunn, J. Barter, B. Green, and R. Bergholtz. Experimental investigation of vane clocking in a one and 1/2 stage high pressure turbine. ASME Paper GT2004-53477, 2004.

[59] D. J. Hall and J. C. Gibbings. Influence of stream turbulences and pressure gradient upon boundary layer transition. *Journal of Mechanical Engineering Science*, **14**:134–146, 1972.

[60] D. E. Halstead, D. C. Wisler, T. H. Okiishi, H. P. Hodson, G. J. Walker, and H-W Shin. Boundary layer development in axial compressors and turbines: Part 4 of 4 — Computations and analyses. *ASME Journal of Turbomachinery*, **119** (1):128–139, 1997.

[61] D. E. Halstead, D. C. Wisler, T. H. Okiishi, G. J. Walker, H. P. Hodson, and H-W Shin. Boundary layer development in axial compressors and turbines. Part 1 of 4: Composite picture. *ASME Journal of Turbomachinery*, **119**(1):114–127, 1997.

[62] D. E. Halstead, D. C. Wisler, T. H. Okiishi, G. J. Walker, H. P. Hodson, and H-W Shin. Boundary layer development in axial compressors and turbines. Part 2 of 4: Compressors. *ASME Journal of Turbomachinery*, **119**(3):426–444, 1997.

[63] D. E. Halstead, D. C. Wisler, T. H. Okiishi, G. J. Walker, H. P. Hodson, and H-W Shin. Boundary layer development in axial compressors and turbines. Part 3 of 4: LP turbines. *ASME Journal of Turbomachinery*, **119**(2):234–246, 1997.

[64] A. Hatman and T. Wang. A prediction model for separated-flow transition. ASME Paper 98-GT-237, 1998.

[65] B. K. Hazarika and C. Hirsch. Transition over C4 leading edge and measurement of intermittency factor using pdf of how-wire signal. *ASME Journal of Turbomachinery*, **119**(3):412–425, 1997.

[66] A. D. Henderson, G. J. Walker, and J. D. Hughes. Influence of free-stream turbulence on wake-wake interaction in an axial compressor. In *Proc. of the 15th Australasian Fluid Mechanics Conference*, The University of Sydney, Australia, 13–17 December 2004. Paper AFMC00086.

[67] A. D. Henderson, G. J. Walker, and J. D. Hughes. Influence of turbulence on wake dispersion and blade row interaction in an axial compressor. *ASME Journal of Turbomachinery*, **128**(1):150–157, 2006.

[68] A. D. Henderson, G. J. Walker, and J. D. Hughes. Unsteady transition phenomena at a compressor blade leading edge. ASME Paper GT2006-90641, 2006.

[69] Y. H. Ho and B. Lakshminarayana. Computation of unsteady viscous flow through turbomachinery blade row due to upstream rotor wakes. *ASME Journal of Turbomachinery*, **117**:541–552, 1995.

[70] G. V. Hobson and R. P. Shreeve. Inlet turbulence distortion and viscous flow development in a controlled-diffusion compressor cascade at very high incidence. *AIAA Journal of Propulsion and Power*, **9**(3):397–404, 1993.

[71] G. V. Hobson, B. E. Wakefield, and W. B. Roberts. Turbulence amplification with incidence at the leading edge of a compressor cascade. *International Journal of Rotating Machinery*, **5**(2):89–98, 1999.

[72] G.V. Hobson, D.J. Hansen, D.G. Schnorenberg, and D.V. Grove. Effect of Reynolds number on separation bubbles on compressor blades in cascade. *AIAA Journal of Propulsion and Power*, **17**(1):154–162, 2001.

[73] H. P. Hodson. Boundary layer and loss measurements on the rotor of an axial-flow turbine. *ASME Journal of Engineering for Gas Turbines and Power*, **106**: 391–399, 1984.

[74] H. P. Hodson. Boundary-layer transition and separation near the leading edge of a high-speed turbine blade. *ASME Journal of Engineering for Gas Turbines and Power*, **107**:127–134, 1985.

[75] H. P. Hodson and R. J. Howell. Bladerow interactions, transition, and high-lift aerofoils in low-pressure turbines. *Annual Review of Fluid Mechanics*, **37**:71–98, 2005.

[76] H. P. Hodson, I. Huntsman, and A. B. Steele. An investigation of boundary layer development in a multistage LP turbine. *ASME Journal of Turbomachinery*, **116** (3):375–383, 1994.

[77] H. P. Hodson and V. Schulte. User guide for PUIM308, University of Cambridge, UK, 1997.

[78] H. P. Horton. A semi-empirical theory for the growth and bursting of laminar separation bubbles. Report CP-1073, Aeronautical Research Council, UK, 1969.

[79] J. Hourmouziadis. Aerodynamic design of low pressure turbines. In *AGARD Lecture Series 167, Blading Design for Axial Turbomachines*, 1989.

[80] M. Howard. Preliminary discussion of CD stator testing program. Private communication to A. D. Henderson, 2004.

[81] A. R. Howell. Private communication to A. R. Oliver, University of Tasmania, 1973.

[82] R. J. Howell, H. P. Hodson, V. Schulte, R. D. Stieger, H-P Schiffer, F. Haselbach, and N. W. Harvey. Boundary layer development in the BR710 and BR715 LP turbines — The implementation of high-lift and ultra-high-lift concepts. *ASME Journal of Turbomachinery*, **124**:385–392, 2002.

[83] J. D. Hughes. *Unsteady Aerodynamics in an Axial Flow Compressor*. PhD thesis, University of Tasmania, Australia, 2001.

[84] J. D. Hughes. Design of a controlled-diffusion stator blade for testing in the UTAS research compressor. Private communication to A. D. Henderson, 2002.

[85] J. D. Hughes and G. J. Walker. Natural transition phenomena on an axial compressor blade. *ASME Journal of Turbomachinery*, **123**:392–401, 2001.

[86] F. Hummel. Wake-wake interaction and its potential for clocking in a transonic high-pressure turbine. *ASME Journal of Turbomachinery*, **124**(1):69–76, 2002.

[87] J. C. R. Hunt and D. J. Carruthers. Rapid distortion theory and the 'problems' of turbulence. *Journal of Fluid Mechanics*, **212**(2):497–532, 1990.

[88] M. Ichimiya, I. Nakamura, and S. Yamashita. Properties of a relaminarizing turbulent boundary layer under a favorable pressure gradient. *Experimental Thermal and Fluid Science*, **17**(1-2):37–48, 1998.

[89] AEA Technology Inc. CFX-5.5.1 documentation, 1998.

[90] R. G. Jacobs and P. A. Durbin. Simulations of bypass transition. *Journal of Fluid Mechanics*, **428**:185–212, 2001.

[91] W. P. Jones and B. E. Launder. The prediction of laminarization with a two equation model of turbulence. *International Journal of Heat and Mass Transfer*, **15**:301–314, 1972.

[92] D. B. M. Jouini, D. Little, E. Bancalari, M. Dunn, C. Haldeman, and P.D. Johnson. Experimental investigation of airfoil wake clocking impacts on aerodynamic performance in a two stage turbine test rig. ASME Paper GT-2003-38872, 2003.

[93] J. M. Kendall. Studies on laminar boundary-layer receptivity to freestream turbulence near a leading edge. In *ASME Fluids Engineering Division (FED)*, volume 114, pages 23–30, 1991.

[94] J. L. Kerrebrock and A. A. Mikolajczak. Intra-stator transport of rotor wakes and its effect on compressor performance. *ASME Journal of Engineering for Power*, **92**(4):359–368, 1970.

[95] P. S. Klebanoff. Contributions on the mechanics of boundary-layer transition. *Bulletin of the American Physical Society*, **10**, 1971.

[96] C. F. Knapp and P. J. Roache. A combined visual and hot-wire anemometer investigation of boundary-layer transition. *AIAA Journal*, **6**(1):29–36, 1968.

[97] U. Köller, R. Mönig, B. Küsters, and H. A. Schreiber. Development of advanced compressor aerofoils for heavy-duty gas turbines — Part 1: Design and optimization. *ASME Journal of Turbomachinery*, **122**:397–405, 2000.

[98] M. Lang, U. Rist, and S. Wagner. Investigations on controlled transition development in a laminar separation bubble by means of LDA and PIV. *Experiments in Fluids*, **36**:43–52, 2004.

[99] R. B. Langtry, F. R. Menter, S. R. Likki, Y. B. Suzen, P. G. Huang, and S. Völker. A correlation-based transition model using local variables — Part II: Test cases and industrial applications. *ASME Journal of Turbomachinery*, **128**: 413–422, 2006.

[100] B. E. Launder. Laminarization of the turbulent boundary layer in a severe acceleration. *ASME Journal of Applied Mechanics*, **31E**:707–708, 1964.

[101] S. Lieblein. Experimental flow in 2D cascades. Technical Report SP 36, NACA, 1965.

[102] S. Lieblein and W. H. Roudebush. Theoretical loss relations for low-speed two-dimensional cascade. Technical Report TN 3662, NACA, 1956.

[103] H. W. Liepmann. Investigation of boundary layer transition on concave walls. Technical Report ACR-4J28, NACA Wartime Rept, 1945.

[104] M. J. Lighthill. A mathematical method of cascade design. Aeronautical Research Council (ARC) Reports and Memoranda 2104, UK, 1945.

[105] H. Liu, B. Liu, L. Li, and H. Jiang. Effect of leading-edge geometry on separation bubble on a compressor blade. ASME Paper GT-2003-38217, 2003.

[106] R. C. Lockhart. *Some Unsteady Flow Phenomena Downstream of an Axial Compressor Stage*. MEngSc Thesis, University of Tasmania, 1973.

[107] R. C. Lockhart and G. J. Walker. The influence of viscous interactions on the flow downstream of an axial compressor stage. In *Proceedings of the 2nd International Symposium on Air Breathing Engines*, Sheffield, UK, 1974.

[108] W. Lou and J. Hourmouziadis. Separation bubbles under steady and periodic-unsteady main flow conditions. *ASME Journal of Turbomachinery*, **122**:634–642, 2000.

[109] L. M. Mack. Transition prediction and linear stability theory. In *AGARD-CP-224*, pages 1.1–1.22, 1977.

[110] R. Mailach and K. Vogeler. Rotor-stator interactions in a four-stage low speed axial compressor — Part 1: Unsteady profile pressures and the effect of clocking. ASME Paper GT2004-53098, 2004.

[111] R. E. Mayle. The role of laminar–turbulent transition in gas turbine engines. *ASME Journal of Turbomachinery*, **113**:509–537, 1991.

[112] R. E. Mayle, K. Dullenkopf, and A. Schultz. The turbulence that matters. *ASME Journal of Turbomachinery*, **120**:402–409, 1998.

[113] B. R. McAuliffe and M. I. Yaras. Numerical study of instability mechanisms leading to transition in separation bubbles. ASME Paper GT2006-91018, 2006.

[114] F. R. Menter, R. B. Langtry, S. R. Likki, Y. B. Suzen, P. G. Huang, and S. Völker. A correlation-based transition model using local variables — Part I: Model formulation. *ASME Journal of Turbomachinery*, **128**:413–422, 2006.

[115] R. X. Meyer. The effect of wakes on the transient pressure and velocity distributions in turbomachines. *Transactions of the ASME*, **80**:1544–1552, 1958.

[116] V. Michelassi, J. G. Wissink, J. Fröhlich, and W. Rodi. Large-eddy simulation of flow around low-pressure turbine blade with incoming wakes. *AIAA Journal*, **41**(11):2143–2156, 2003.

[117] M. V. Morkovin. On the many faces of transition. In Sinclair C. Wells, editor, *Symposium on Viscous Drag Reduction*, LTV Research Center, Dallas, Texas, USA, 1968.

[118] R. Narashimha, K. J. Devasia, G. Gururani, and M. A. Badri Narayanan. Transitional intermittency in boundary layers subjected to pressure gradient. *Experiments in Fluids*, **2**:171–176, 1984.

[119] R. Narasimha and K. Sreenivasan. Relaminarization of fluid flows. *Advances in Applied Mechanics*, **19**:221–309, 1979.

[120] Advisory Group for Aerospace Research and Development. North Atlantic Treaty Organization (NATO). A portfolio of stability characteristics for incompressible boundary layers. AGARDograph 134, 1969.

[121] H. J. Obremski and A. A. Fejer. Transition in oscillating boundary layer flows. *Journal of Fluid Mechanics*, **29**(1):93–111, 1967.

[122] A. R. Oliver. Comparison between sand cast and machined blades in the vortex wind tunnel. Aeronautical Research Laboratories (ARL) Report ME.103, Australia, 1961.

[123] A. R. Oliver. Private communication to A. D. Henderson, University of Tasmania, 1999.

[124] P. L. O'Neill, D. Nicolaides, D. Honnery, and J. Soria. Autocorrelation functions and the determination of integral length with reference to experimental and numerical data. In *Proc. of the 15th Australasian Fluid Mechanics Conference*, The University of Sydney, Australia, 13-17 December 2004.

[125] M. M. Opoka and H. P. Hodson. An experimental investigation of the unsteady transition process on the high lift T106A turbine blade. ISABE Paper 2005-1277, 2005.

[126] M. M. Opoka, R. L. Thomas, and H. P. Hodson. Boundary layer transition on the high lift T106A LP turbine blade with an oscillating downstream pressure field. ASME Paper GT2006-91038, 2006.

[127] U. Orth. Unsteady boundary-layer transition in flow periodically disturbed by wakes. *ASME Journal of Turbomachinery*, **115**:707–713, 1993.

[128] V. C. Patel and M. R. Head. Reversion of turbulent to laminar flow. *Journal of Fluid Mechanics*, **34**:371–392, 1968.

[129] D. E. Paxson and R. E. Mayle. Laminar boundary layer interaction with an unsteady passing wake. *ASME Journal of Turbomachinery*, **113**:419–427, 1991.

[130] H. Pfeil, R. Herbst, and T. Schröder. Investigation of the laminar-turbulent transition of boundary layers disturbed by wakes. *ASME Journal of Engineering for Power*, **105**:130–137, 1983.

[131] J. M. M. Place, M. A. Howard, and N. A. Cumpsty. Simulating the multi-stage environment for single-stage compressor experiments. *ASME Journal of Turbomachinery*, **118**:706–716, 1996.

[132] J. H. Preston. The minimum Reynolds number for a turbulent boundary layer and the selection of a transition device. *Journal of Fluid Mechanics*, **3**:373–384, 1957.

[133] U. Reinmöller, B. Stephan, S. Schmidt, and R. Niehuis. Clocking effects in a 1.5 stage axial turbine — Steady and unsteady experimental investigations supported by numerical simulations. *ASME Journal of Turbomachinery*, **124** (1):52–60, 2002.

[134] H. G. Rhoden. Effects of Reynolds number on the flow of air through a cascade of compressor blades. Report 2919, Aeronautical Research Council R and M, 1952.

[135] P. E. Roach. The generation of nearly isotropic turbulence by means of grids. *International Journal of Heat and Fluid Flow*, **8**(2):82–92, 1987.

[136] S. K. Roberts and M. I. Yaras. Large-eddy simulation of transition in a separation bubble. ASME Paper GT2005-68666, 2005.

[137] S. K. Roberts and M. I. Yaras. Modeling transition in separated and attached boundary layers. *ASME Journal of Turbomachinery*, **127**(2):402–411, 2005.

[138] W. B. Roberts. Calculation of laminar separation bubbles and their effect on airfoil performance. *AIAA Journal*, **18**(1):25–31, 1980.

[139] W. B. Roberts. Advanced turbofan blade refurbishment technique. *ASME Journal of Turbomachinery*, **117**:666–667, 1995.

[140] L. Rosenhead. Laminar boundary layers. In *The Fluid Motion Memoirs*. Oxford at Clarendon Press, 1963.

[141] N. L. Sanger and R. P. Shreeve. Comparison of calculated and experimental cascade performance for controlled-diffusion compressor stator blading. *ASME Journal of Turbomachinery*, **108**:42–50, 1986.

[142] W. S. Saric, H. L. Reed, and E. J. Kerschen. Boundary-layer receptivity to freestream disturbances. *Annual Review of Fluid Mechanics*, **34**:291–319, 2002.

[143] S. Sarkar and P. R. Voke. Large-eddy simulation of unsteady surface pressure over a low-pressure turbine blade due to interactions of passing wakes and inflexional boundary layer. *ASME Journal of Turbomachinery*, **128**:221–231, 2006.

[144] A. M. Savill. By-pass transition using conventional closures. In B. E. Launder and Sandham N. D., editors, *Closure Strategies for Turbulent and Transitional Flows*, pages 464–492. Cambridge University Press, 2002.

[145] A. M. Savill. New strategies in modelling by-pass transition. In B. E. Launder and Sandham N. D., editors, *Closure Strategies for Turbulent and Transitional Flows*, pages 493–521. Cambridge University Press, 2002.

[146] H. Schlichting. Zur entstehung der turbulenz bei der plattenströmung. Z. Angew. Math. Mech. 13:260-263, 1933.

[147] H. Schlichting. *Boundary-Layer Theory*. McGraw–Hill, 6th edition, 1968.

[148] R. C. Schmidt and S. V. Patankar. Simulating boundary layer transition with low-Reynolds-number k-ϵ turbulence models: Part 1 — An evaluation of prediction characteristics. *ASME Journal of Turbomachinery*, **113**:10–17, 1991.

[149] R. C. Schmidt and S. V. Patankar. Simulating boundary layer transition with low-Reynolds-number k-ϵ turbulence models: Part 2 — An approach to improving the predictions. *ASME Journal of Turbomachinery*, **113**:18–26, 1991.

[150] G. B. Schubauer and P. S. Klebanoff. Contributions on the mechanics of boundary-layer transition. NACA Technical Report 1289, 1956.

[151] V. Schulte and H. P. Hodson. Unsteady wake-induced boundary layer transition in high lift LP turbines. *ASME Journal of Turbomachinery*, **120**:28–35, 1998.

[152] A. M. O. Smith and N. Gamberoni. Transition, pressure gradient, and stability theory. Report ES 26388, Douglas Aircraft Co., 1956.

[153] L. H. Smith, Jr. Wake dispersion in turbomachines. *ASME Journal of Basic Engineering Science*, **88**:688–690, 1966.

[154] W. J. Solomon. *Unsteady Boundary Layer Transition on Axial Compressor Blades*. PhD thesis, University of Tasmania, Australia, 1996.

[155] W. J. Solomon and G. J. Walker. Observations of wake-induced transition on an axial compressor blade. ASME Paper 95-GT-381, 1995.

[156] W. J. Solomon and G. J. Walker. Incidence effects on wake -induced trasnition on an axial compressor blade. *AIAA Journal of Propulsion and Power*, **16**: 397–405, 2000.

[157] W. J. Solomon, G. J. Walker, and J. P. Gostelow. Transition length prediction for flows with rapidly changing pressure gradients. *ASME Journal of Turbomachinery*, **118**(4):744–751, 1996.

[158] W. J. Solomon, G. J. Walker, and J. D. Hughes. Periodic transition on an axial compressor stator: Incidence and clocking effects: Part II — Transition onset predictions. *ASME Journal of Turbomachinery*, **121**:408–415, 1999.

[159] F. Soranna, Y. Chow, O. Uzol, and J. Katz. The effect of IGV wake impingement on the flow structure and turbulence around a rotor blade. *ASME Journal of Turbomachinery*, **128**(1):82–95, 2006.

[160] K. R. Sreenivasan. Laminarescent, relaminarizing and retransitional flows. *ACTA MECHANICA*, **44**:1–48, 1982.

[161] J. Steelant and E. Dick. Modelling of bypass transition with conditioned Navier–Stokes equations coupled to an intermittency transport equation. *International Journal for Numerical Methods in Fluids*, **23**:193–220, 1996.

[162] R. D. Stieger and H. P. Hodson. The transition mechanism of highly-loaded LP turbine blades. ASME Paper GT2003-38304, 2003.

[163] R. D. Stieger and H. P. Hodson. The unsteady development of a turbulent wake through a downstream low-pressure turbine blade passage. *ASME Journal of Turbomachinery*, **127**(2):388–394, 2005.

[164] R. D. Stieger, D. Hollis, and H. P. Hodson. Unsteady surface pressures due to wake-induced transition in a laminar separation bubble on a low-pressure cascade. *ASME Journal of Turbomachinery*, **126**:544–550, 2004.

[165] Y. B. Suzen and P. G. Huang. Numerical simulation of unsteady wake/blade interactions in low-pressure turbine flows using an intermittency transport equation. *ASME Journal of Turbomachinery*, **127**:431–444, 2005.

[166] L. Tain. *Compressor Leading Edges in Incompressible and Compressible Flows*. PhD thesis, Cambridge University, UK, 1998.

[167] L. Tain and N. A. Cumpsty. Compressor blade leading edges in subsonic compressible flow. *Journal of Mechanical Engineering Science*, **214**(1):221–242, 2000.

[168] R. L. Thomas and J. P. Gostelow. The pervasive effect of the calmed region. ASME Paper GT2005-69125, 2005.

[169] M. Tiedemann and F. Kost. Some aspects of wake-wake interactions regarding turbine stator clocking. *ASME Journal of Turbomachinery*, **123**(3):526–533, 2001.

[170] W. Tollmien. Über die entstehung der turbulenz. Nachr. Ges. Wiss, Göttingen, Math. Phys. Klasse 1:21-44, 1929.

[171] D. J. Tritton. *Physical Fluid Dynamics*. Clarendon Press, Oxford, 2nd edition, 1988.

[172] J. L. van Ingen. A suggested semi-empirical method for the calculation of the boundary layer transition region. In *Proceedings of the Second European Aeronautical Congress*, pages 37.1–37.16, Scheveningen, 1956.

[173] S. Vilmin, H. P. Hodson, W. N. Dawes, and A. M. Savill. Predicting wake-passing transition in turbomachinery using an intermittency-conditioned modelling approach. ERCOFTAC Bulletin 54, 2002.

[174] P. Voke, Yang Z., and A. M. Savill. Large-eddy simulation and modelling of transition following a leading-edge separation bubble. In W. Rodi and G. Bergeles, editors, *Engineering Turbulence Modelling and Experiments 3. Proceedings of The Third International Symposium on Engineering Turbulence Modelling and Measurements*, pages 601–610, Herkalion-Crete, Greece, 1996. Elsevier.

[175] G. J. Walker. *An Investigation of the Boundary Layer Behavour on the Blading of a Single-Stage Axial-Flow Compressor*. PhD thesis, University of Tasmania, 1972.

[176] G. J. Walker. Transitional flow on axial turbomachine blading. *AIAA Journal*, **27**(5):595–602, 1989.

[177] G. J. Walker. The role of laminar–turbulent transition in gas turbine engines: A discussion. *ASME Journal of Turbomachinery*, **117**:207–217, 1993.

[178] G. J. Walker. Laminar-turbulent transition in aerofoil flows. In M. Alam, Rama Govindarajan, O. N. Ramesh, and K. R. Sreenivas, editors, *Symposium on Advances in Fluid Mechanics*, Bangalore, India, 2003.

[179] G. J. Walker and J. P. Gostelow. Effects of adverse pressure gradients on the nature and length of boundary layer transition. *ASME Journal of Turbomachinery*, **112**:196–205, 1990.

[180] G. J. Walker, J. D. Hughes, I. Köhler, and W. J. Solomon. The influence of wake-wake interactions on loss fluctuations of a downstream axial compressor blade row. *ASME Journal of Turbomachinery*, **120**:695–704, 1998.

[181] G. J. Walker, J. D. Hughes, and W. J. Solomon. Periodic transition on an axial compressor stator: Incidence and clocking effects: Part I — Experimental data. *ASME Journal of Turbomachinery*, **121**:398–407, 1999.

[182] R. E. Walraevens and N. A. Cumpsty. Leading edge separation bubbles on turbomachine blades. *ASME Journal of Turbomachinery*, **117**:115–126, 1995.

[183] D. Warnack and H. H. Fernholz. The effects of a favourable pressure gradient and of the Reynolds number on an incompressible axisymmetric turbulent boundary layer. Part 2. The boundary layer with relaminarization. *Journal of Fluid Mechanics*, **359**:357–381, 1998.

[184] D. Warnack and H. H. Fernholz. The effects of a favourable pressure gradient and of the Reynolds number on an incompressible axisymmetric turbulent boundary layer. Part 2. The boundary layer with relaminarization. *Journal of Fluid Mechanics*, **359**:357–381, 1998.

[185] K. J. A. Westin, A. A. Bakchinov, V. V. Kozlov, and P. H. Alfredsson. Experiments on localized disturbances in a flat plate boundary layer. Part 1. The receptivity and evolution of a localized free stream disturbance. *European Journal of Mechanics B/Fluids*, **17**(6):823–846, 1998.

[186] K. J. A. Westin, A. V. Boiko, B. G. B. Klingmann, V. V. Kozlov, and P. H. Alfredsson. Experiments in a boundary layer subjected to free stream turbulence. Part 1. Boundary layer structure and receptivity. *Journal of Fluid Mechanics*, **281**:193–218, 1994.

[187] A. P. S. Wheeler, R. J. Miller, and H. P. Hodson. The effect of wake-induced structures on compressor boundary layers. ASME Paper GT2006-90892, 2006.

[188] F. M. White. *Viscous Fluid Flow*. McGraw–Hill, 1974.

[189] D. C. Wisler. Loss reduction in axial-flow compressors through low-speed model testing. *ASME Journal of Turbomachinery*, **107**:354–363, 1985.

[190] D. C. Wisler, R. C. Bauer, and T. H. Okiishi. Secondary flow, turbulent diffusion, and mixing in axial flow compressors. *ASME Journal of Turbomachinery*, **109**: 455–482, 1987.

[191] D. C. Wisler, D. E. Halstead, and B. F. Beacher. Improving compressor and turbine performance through cost-effective low-speed testing. ISOBE Paper 99-7073, 1999.

[192] A. W. Wright and E. Szomanski. Calibration of the vortex wind tunnel. Aeronautical Research Laboratories (ARL), Report ME.165, Australia, 1956.

[193] X. Wu and P. A. Durbin. Boundary layer transition induced by periodic wakes. *ASME Journal of Turbomachinery*, **122**:442–448, 2000.

[194] X. Wu, R. G. Jacobs, J. C. R. Hunt, and P. A. Durbin. Simulations of boundary layer transition induced by periodically passing wakes. *Journal of Fluid Mechanics*, **398**:109–153, 1999.

[195] Z. Yang and P. R. Voke. Large eddy simulation of boundary-layer separation and transition at a change of surface curvature. *Journal of Fluid Mechanics*, **439**:305–333, 2001.

[196] T. A. Zaki and P. A. Durbin. Mode interaction and the bypass route to transition. *Journal of Fluid Mechanics*, **531**:85–111, 2005.

[197] T. A. Zaki, P. A. Durbin, J. Wissink, and W. Rodi. Direct numerical simulation of by-pass and separation-induced transition in a linear compressor cascade. ASME Paper GT2006-90885, 2006.

[198] S. Zhong, T. P. Chong, and H. P. Hodson. A comparison of spreading angles of turbulent wedges in velocity and thermal boundary layers. *Journal of Fluid Mechanics*, **125**:267–274, 2003.

[199] S. Zhong, C. Kittichaikan, H. P. Hodson, and P. T. Ireland. Visualisation of turbulent spots and unsteady wake-induced boundary-layer transition with thermochromic crystals. *Optics and Laser Technology*, **31**(1):33–39, 1999.

[200] W. C. Zierke and S. Deutsch. The measurement of boundary layers on a compressor blade in cascade: Part 4 — Flow fields for incidence angles of -1.5 and -8.5 degrees. *ASME Journal of Turbomachinery*, **112**:241–255, 1990.

[201] Y. Zohar and C. M. Ho. Dissipation scale and control of fine-scale turbulence in a plane mixing layer. *Journal of Fluid Mechanics*, **320**:139–161, 1996.